CONF-9606178--1

Janis A. Keeney,[1] B. Richard Bass,[1] and Wallace J. McAfee[1]

FRACTURE ASSESSMENT OF WELD MATERIAL FROM A FULL-THICKNESS CLAD RPV SHELL SEGMENT

REFERENCE: Keeney, J. A., Bass, B. R., and McAfee, W. J., "**Fracture Assessment of Weld Material From a Full-Thickness Clad RPV Shell Segment,**" Fatigue and Fracture Mechanics: 28th Volume, ASTM STP 1321, J. H. Underwood, B. D. Macdonald, and M. R. Mitchell, Eds., American Society for Testing and Materials, 1997.

ABSTRACT: Fracture analysis techniques were evaluated through applications to full-thickness clad beam specimens containing shallow cracks in material for which metallurgical conditions are prototypic of those found in reactor pressure vessels (RPVs) at beginning of life. The beam specimens were fabricated from a section of an RPV wall (removed from a canceled nuclear plant) that includes weld, plate, and clad material. Metallurgical factors potentially influencing fracture toughness for shallow cracks in the beam specimens include gradients of material properties and residual stresses due to welding and cladding applications. Fracture toughness estimates were obtained from load vs load-line displacement and load vs crack-mouth-opening displacement data using finite-element techniques and estimation schemes based on the η-factor method. One of the beams experienced a significant amount of precleavage stable ductile tearing. Effects of precleavage tearing on estimates of fracture toughness were investigated using continuum damage models. Fracture toughness results from the clad beam specimens were compared with other deep- and shallow-crack single-edge notch bend (SENB) data generated previously from A 533 Grade B plate material. The range of scatter for the clad beam data is consistent with that from the laboratory-scale SENB specimens tested at the same temperature.

KEYWORDS: reactor pressure vessel, full-thickness clad beams, shallow-crack, single-edge notch bend specimens, constraint, η-factor method, J-Q methodology, crack-tip stress triaxiality, precleavage tearing, continuum damage models

Evaluations of reactor pressure vessel (RPV) integrity under pressurized-thermal shock (PTS) loading are based on the Marshall flaw distribution [1], U.S. Nuclear Regulatory Commission (NRC) Guide 1.154 [2], and data from deep-crack fracture toughness specimens. The Marshall flaw distribution predicts more small (shallow) than large (deep) flaws, while NRC Regulatory Guide 1.154 requires that all flaws be

[1]Engineers, Oak Ridge National Laboratory, P. O. Box 2009, Oak Ridge, TN 37831-8056.

considered as surface flaws. Probabilistic fracture-mechanics (PFM) analyses of RPVs indicate that a high percentage of the cracks that initiate in cleavage, initiate from shallow flaws [3]. Because the postulated existence of shallow flaws has a dominant influence on the results of PFM analyses and, ultimately, the conditional probability of vessel failure in a PTS evaluation, the shallow surface crack is of major importance in RPV structural integrity assessments.

Fracture analysis techniques were used to investigate results from a Heavy-Section Steel Technology (HSST) testing program designed to quantify fracture toughness for shallow cracks in weld material for which metallurgical conditions are prototypic of those found in RPVs at beginning of life. In the first phase of the investigation, five full-thickness clad beam specimens taken from the RPV of a canceled nuclear plant were fabricated at Oak Ridge National Laboratory (ORNL) and tested at the National Institute for Standards and Technology (NIST), Gaithersburg, Maryland. These tests were performed to determine the influence of material properties gradients, weld inhomogeneities, weld defects and the cladding process on the fracture toughness of material containing shallow cracks. Through-clad shallow cracks in these beams were machined in the weld material joining together two plate material shell segments. Comparison of results from these tests with those from homogeneous shallow-crack test specimens [4] provide an opportunity to quantify effects of some near surface conditions on fracture toughness. Also, the clad beam data were used to evaluate the stress-based constraint characterizations developed by O'Dowd and Shih [5-7].

FULL-THICKNESS CLAD BEAM TESTING PROGRAM

Details of Test Specimen

The full-thickness clad beam specimens were fabricated from an RPV shell segment that was available from a canceled pressurized-water reactor plant (the plant was canceled during construction, and the vessel was never in service). The RPV material is A 533 B steel with a stainless steel clad overlay on the inner surface. The shell segment contains three submerged-arc welds (two circumferential welds and one longitudinal weld). The plate material, clad overlay, and weldment are completely prototypic of a production-quality RPV.

Because the first series of five specimens was intended to investigate the fracture behavior of the longitudinal weld material, the test beams were cut in the circumferential direction of the shell. A sketch of the specimen geometry is shown in Fig. 1. The specimen was designed to be tested in three-point bending. The flaw was machined in the beam using the wire electro-discharge machining process and extended from the shell inner surface, that is, the clad surface, to predetermined depths into the beam. The final dimensions for each clad beam specimen are shown in Table 1. One deep-flaw specimen (CB-1.1) and four shallow-flaw specimens (CB-1.2 – CB-1.5) were produced.

Impact and tensile data were used to develop a consistent set of material properties needed for the clad beam test data evaluation and the finite-element analyses. These properties are listed in Table 2. The tabulated yield stress for the weld material is 36% higher than the yield stress for the base material.

Test Procedures and Results

The full-thickness clad beam tests were instrumented with crack-mouth-opening displacement (CMOD) and load-line displacement (LLD) gages and tested in three-point bending. Each specimen was cooled to the test temperature [–25°C (T-NDT=25°C)] and then loaded to fracture in displacement control. Details of the test procedures are described in Refs. 8 and 9. The load (P) vs displacement curves for each of the five beams are

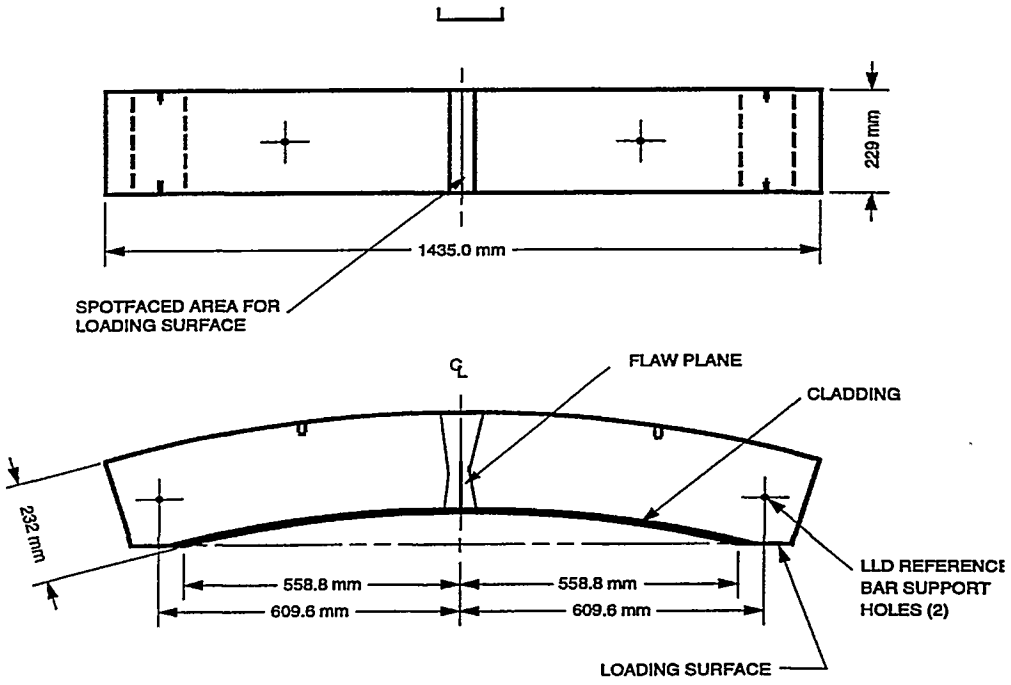

FIG. 1--Sketch of full-thickness clad beam specimen.

TABLE 1--Parameters defining specimen geometry of full-thickness clad beam specimens.

	CB-1.1[a]	CB-1.2	CB-1.3	CB-1.4	CB-1.5
Load span, S (mm)	1219.2	1219.2	1219.2	1219.2	1219.2
Thickness[b], B (mm)	230.2	230.2	229.6	229.1	231.6
Width, W (mm)	225.7	224.3	224.3	228.9	225.0
Crack depth[c], a (mm)	117.5	10.8	23.7	22.6	12.1
Ratio, a/W	0.50	0.05	0.10	0.10	0.05

[a]Used as development beam.
[b]Thickness includes ~5 mm of clad overlay.
[c]Final depth after fatigue precracking.

TABLE 2--Material properties at test temperature of –25°C

	Base metal	Weld metal	Cladding
Modulus of elasticity (E), MPa	200,000	200,000	152,000
Poisson's ratio (ν)	0.3	0.3	0.3
Yield stress (σ_0), MPa	440	599	367
Ultimate stress (σ_u), MPa	660	704	659
RT_{NDT}, °C		–23	
NDT, °C	–34	–50	

shown in Fig. 2(a) for LLD and in Fig. 2(b) for CMOD, respectively. These curves depict the inelastic behavior in the shallow-crack specimens as fracture conditions are approached as compared to the near elastic conditions for the deep-crack specimen. The conditions of each specimen at failure are listed in Table 3, including the plastic component of the area under the P vs displacement curve (defined as U_{pl} for LLD and A_{pl} for CMOD).

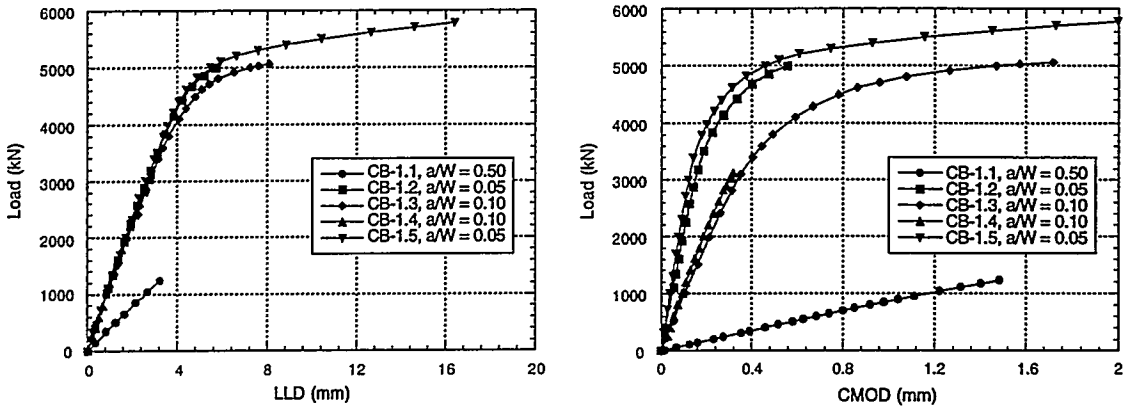

FIG. 2--Load vs displacement response for clad beam specimens: (a) LLD and (b) CMOD.

TABLE 3--Summary of results from the full-thickness clad beam testing program.

	CB-1.1	CB-1.2	CB-1.3	CB-1.4	CB-1.5
a/W	0.50	0.05	0.10	0.10	0.05
Temperature, °C	-25.5 ± 1.0	-25.0 ± 1.0	-25.0 ± 1.0	-25.3 ± 1.0	-25.9 ± 1.0
Stroke Rate, mm/min.	2.49	8.38	6.89	3.76	8.76
Time to Failure, s	230	366	440	309	556
Failure conditions					
P, kN	1232.5	5002.3	5060	3114	5783
LLD, mm	3.236	5.767	8.083	2.825	16.396
CMOD, mm	1.485	0.567	1.718	0.318	1.998
U_{pl}, kN-mm	135	6427	16879	93	—[a]
A_{pl}, kN-mm	88	1473	5486	79	—[a]

[a]Not calculated since CB-1.5 underwent precleavage ductile tearing and toughness was not estimated using η-factors.

CLAD BEAM POSTTEST ANALYSES

Finite-Element Analysis

Two different analysis techniques were used to generate finite-element solutions for the full-thickness clad beam tests. In clad beam tests CB-1.1 – CB-1.4, the cracks initiated in cleavage thus allowing the use of static analysis techniques. The CB-1.5 specimen experienced ~2.6 mm of stable ductile tearing prior to initiation of cleavage fracture. Recent studies indicate that the onset of stable ductile tearing leads to crack-tip fields ahead of the growing crack and crack-tip profiles that differ from those of a stationary crack. Stable ductile tearing exposes additional volumes of material to elevated stresses as the crack advances, which alters the sampling of potential cleavage initiation sites on the

microstructural level. Also, measured cleavage fracture toughness values for these specimens will be influenced by changes in crack-tip constraint conditions that occur with prior stable crack growth. The analysis of CB-1.5 utilized the Gurson-Tvergaard (G-T) dilatant plasticity model [10] for void growth and element extinction capability for modeling crack growth.

Cleavage Model--Two-dimensional (2-D) plane-strain elastic-plastic analyses were performed on the clad beam specimens (CB-1.1 – CB-1.4) using ABAQUS [11]. A one-half section of the complete clad beam specimen illustrated in Fig. 1 is represented in the 2-D finite-element model of Fig. 3 (a/W = 0.10). The model in Fig. 3 incorporates the curvature of the plate and the flat cut-out where the specimen is supported during loading. The model has a highly refined mesh in the crack-tip region [Fig. 3(c)] to provide resolution of stress fields in front of the crack. The model consists of 3630 nodes and 1105 eight-node isoparametric elements with reduced integration. Collapsed-prism elements arranged in a focused fan configuration at the crack tip are used to produce a 1/r strain singularity appropriate for inelastic analysis. The finite-element model is loaded by a distributed pressure load over four elements on the outer edge [see Fig. 3(b)].

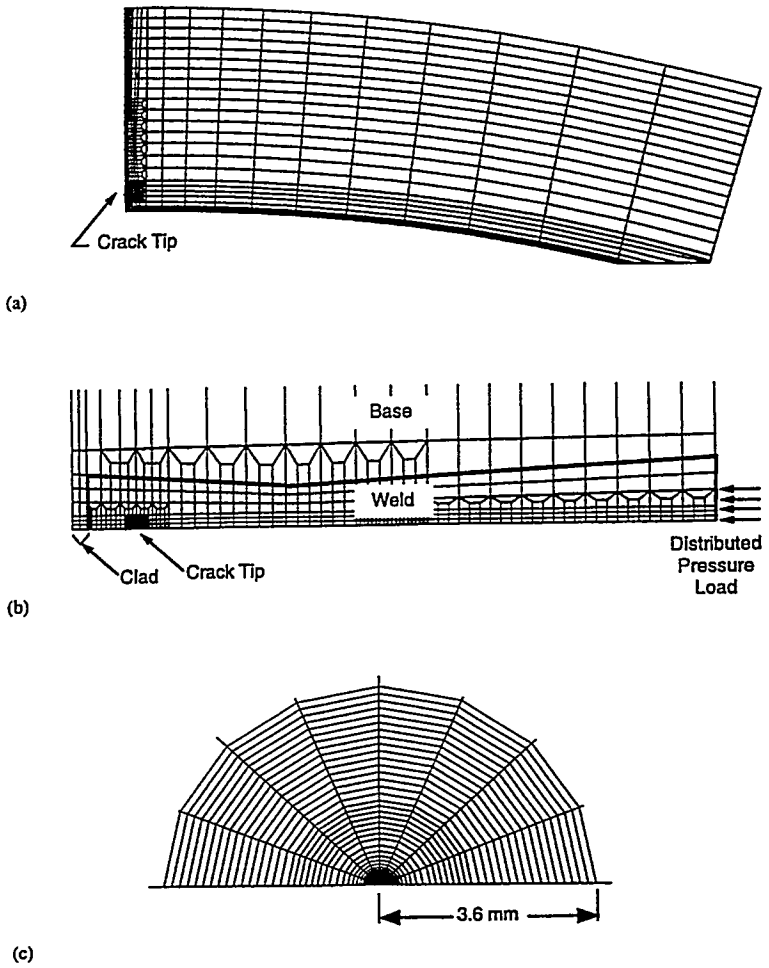

FIG. 3--(a) Finite-element mesh of clad beam specimen with a/W = 0.10, (b) crack-plane region, and (c) crack-tip region

Precleavage Ductile Tearing Model--The finite-element model shown in Fig. 4 was employed to perform plane-strain, nonlinear analyses of the clad beam specimen CB-1.5 (a/W = 0.05) which had a small amount of precleavage ductile tearing (~2.6 mm). The finite-element computer code WARP3D [12] was used to perform the analysis. For 2-D plane-strain analyses, the WARP3D code utilizes a 3-D model with one layer of elements in the thickness direction with plane-strain constraints imposed in the thickness direction on all nodes. The G-T model implemented in WARP3D incorporates void nucleation and growth ahead of a stably tearing crack into a finite-element model using computational cells with explicit length scales. In Fig. 4, the model has 2706 nodes and 1248 elements (8-node bricks). Symmetry about the crack plane permits modeling of one half of the specimen. Square elements in the crack-tip region and along the crack plane are defined to permit uniform increments of crack extension. The crack-tip element size is 100 μm (chosen from prior analytical experience in Ref. 13) for adequate resolution of the crack opening profile and stresses ahead of the growing crack.

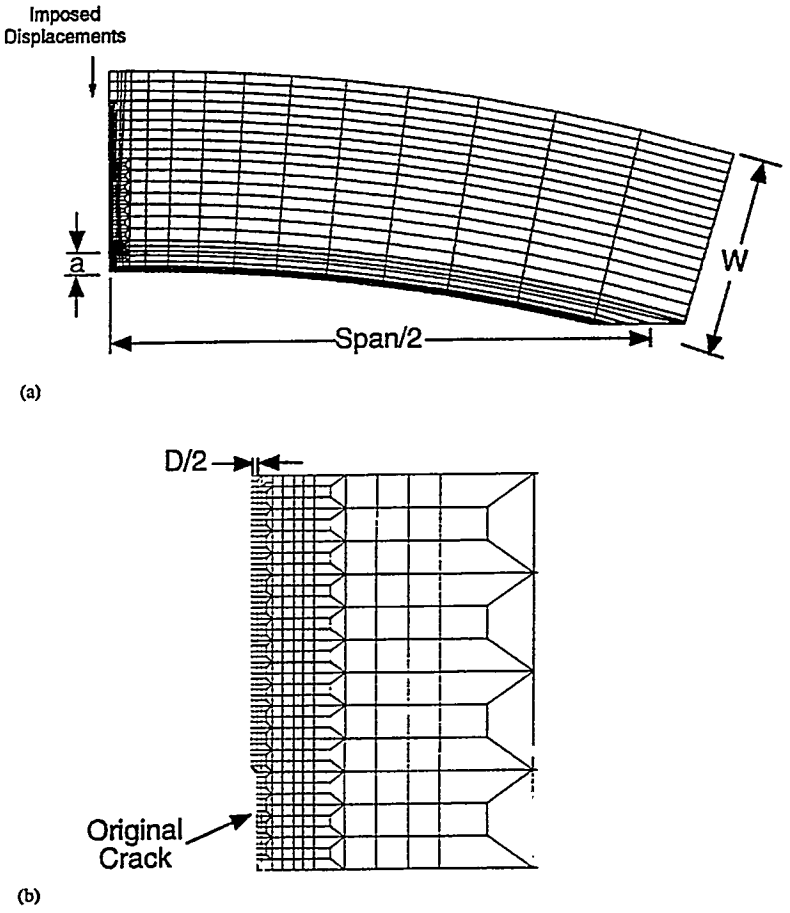

FIG. 4--(a) Finite-element mesh of clad beam specimen CB-1.5 (a/W = 0.05), and (b) crack-plane region

The finite-element model is loaded by displacement increments imposed on six centerplane nodes (the two end elements) as shown in Fig. 4(a). The Gurson constitutive model is used for the elements along the crack plane where ductile tearing occurs, and the rest of the model uses the von Mises constitutive relation. Two principal input parameters for the G-T model are the initial void volume fraction, f_0, and the characteristic length, D,

associated with the G-T crack plane elements. According to theory, these parameters are dependent only on the material and not on specimen geometry. Experimental J-Δa curves obtained from compact specimens can be used to calibrate f_0 and D for the test material. In the absence of these data, a parametric study was performed to obtain the initial volume fraction f_0 and displacement increment which would reproduce the experimental load vs CMOD curve for CB-1.5. The value of f_0 used in the final analysis was 0.006 with a displacement increment of 0.00215 in. The explicit length scale D was set at 200 μm (since the crack-tip element size is 100 μm). The critical volume fraction, set at $f_f = 0.15$, is when void coalescence occurs. Full interpretation of the test results from CB-1.5 has not been completed. Additional work is on-going as noted later in this paper.

Material properties used for the posttest analyses of the clad beam specimens were taken from Table 2 and from the multilinear true stress vs true plastic-strain curves given in Fig. 5.

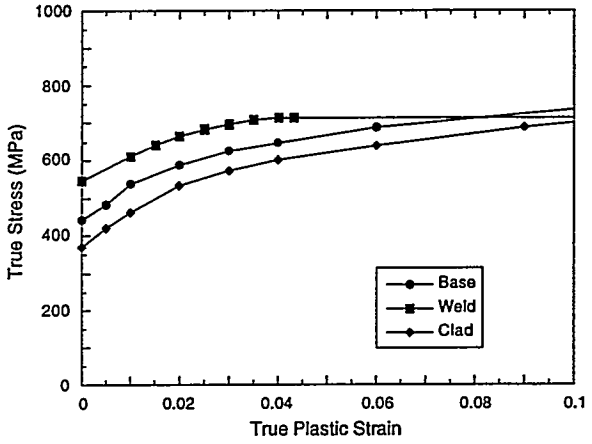

FIG. 5-- Material representation for clad beam at T = –25°C

Finite Element Results

Results from the posttest analyses of the clad beam tests are summarized in Fig. 6(a) and (b). Comparison of the measured and calculated P vs displacement responses provides a way to interpret the accuracy of the analysis results and to establish confidence in the calculated fracture mechanics parameters. The calculated P vs LLD curves are compared with measured data for each test in Fig. 6(a). For the shallow-crack specimens,

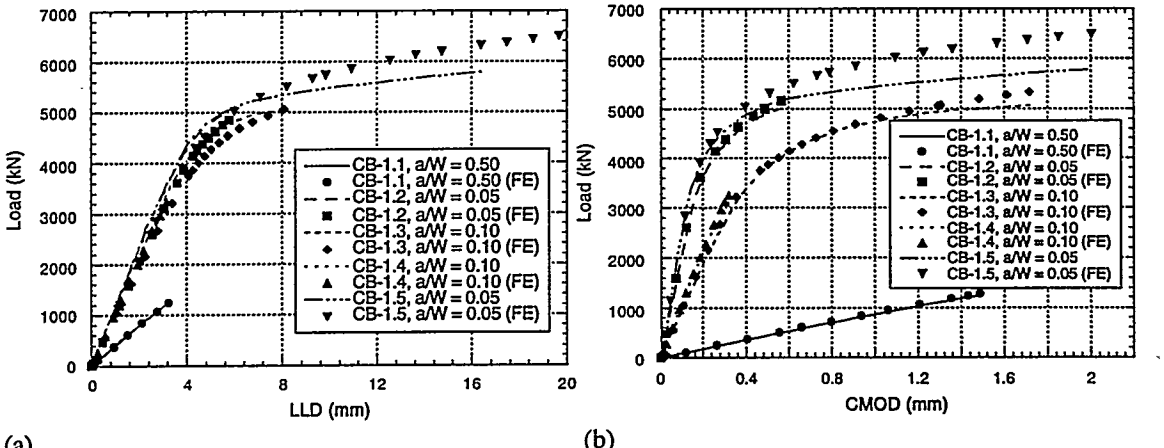

(a) (b)

FIG. 6--Comparison of calculated and measured displacements for clad beam specimens: (a) LLD and (b) CMOD.

calculated LLD values at a given load were greater than measured values for the full range of loading, except CB-1.5 where the measured values of LLD are greater than the calculated values at a given load over the plastic range of loading. Comparisons of calculated and measured P vs CMOD in Fig. 6(b) show good agreement for CB-1.1 – CB-1.4. To match the measured CMOD for CB-1.5, the load had to be increased by 12%. A higher load had to be used because the 3-D plane-strain model is too stiff for an exact comparison between measured and calculated P vs CMOD. Analysis results of CB-1.5, shown in Fig. 7, indicate that the crack began tearing at a load of 5659 kN (J value of 373 kN/m). The crack extended 2.6 mm with an end load of 6497 kN and J value of 1083 kN/m.

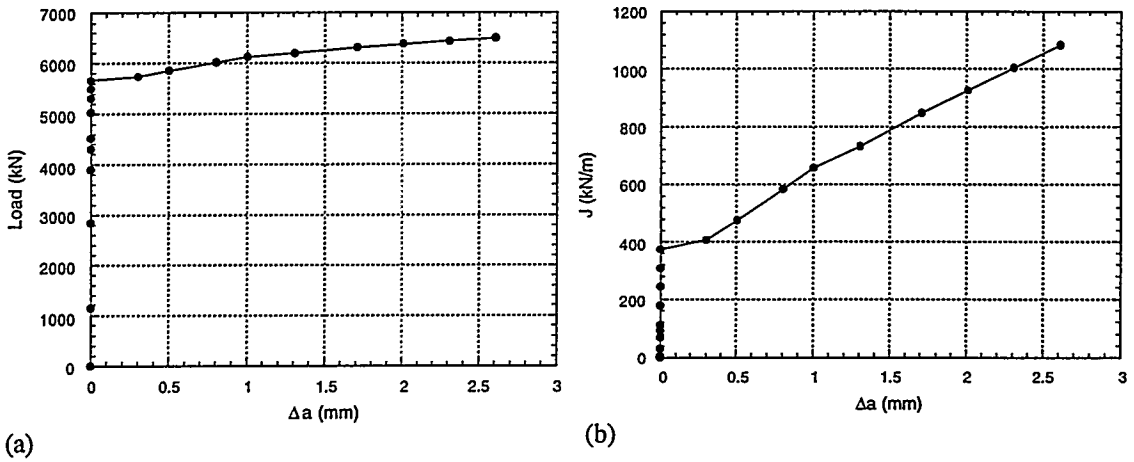

FIG. 7--Analysis results for clad beam specimen CB-1.5: (a) L vs Δa and (b) J vs Δa.

Toughness Estimation Techniques

The two techniques [4, 14, and 15] used to determine the critical J-integral for CB-1.1 – CB-1.4 (initiated in cleavage) are based on the "work" at the crack tip as measured by the area under the load–displacement curves. The methods require an η-factor, which relates work at the crack tip to the plastic portion of the crack-driving force. The first method of estimating J uses the P vs LLD test record. The J-integral is divided into elastic and plastic terms given by

$$J = J_{el} + J_{pl} \ , \tag{1}$$

where

$$J_{pl} = \left(\eta_{pl}^{\ell} U_{pl}\right) / Bb, \tag{2}$$

and U_{pl} is the plastic component of the area under the P vs LLD curve, B is specimen thickness, b is the remaining ligament (W-a), and η_{pl}^{ℓ} is the dimensionless constant relating the area term (U_{pl}) to J_{pl}. Finite-element analysis provides values of η_{pl}^{ℓ} as a function of U_{pl} for each loading and specimen configuration. The U_{pl} value from the measured P vs LLD curve and the corresponding value of η_{pl}^{ℓ} for each test at cleavage initiation are included in Table 4. The second technique for determining the critical J-integral [16] uses

TABLE 4--Summary of analysis results from the full-thickness clad beam testing program.

	CB-1.1	CB-1.2	CB-1.3	CB-1.4	CB-1.5
a/W	0.50	0.05	0.10	0.10	0.05
η-factors					
η_{pl}^{ℓ}	1.37	0.79	1.05	1.69	—
η_{pl}^{c}	2.26	4.16	4.08	2.82	—
Fracture toughness					
Elastic component					
J_{el}, kN/m	131.3	110.6	230.5	73.52	151.6[a]
K_I, MPa$\sqrt{m}$	173.0	154.5	223.1	126.0	180.9
P vs CMOD					
J_{pl}, kN/m	8.1	124.7	486.0	4.69	
Total J, kN/m	139.4	235.3	716.5	78.21	1082.5[b]
K_{Jc}, MPa$\sqrt{m}$	173.5	225.4	393.3	130.0	483.5
P vs LLD					
J_{pl}, kN/m	7.4	103.8	384.8	3.31	—
Total J, kN/m	138.7	214.4	615.3	76.83	—
K_{Jc}, MPa$\sqrt{m}$	173.1	215.2	364.5	128.8	—

[a]Static analysis for crack depth location after ductile tearing (a ~ 14.7 mm).

[b]Gurson-Tvergaard plasticity model for void growth and element extinction for crack growth.

the plastic component of the area under the P vs CMOD curve (A_{pl}) to calculate J_{pl}. The values of A_{pl} (from measured P vs CMOD data) and η_{pl}^{c} for each test at initiation are listed in Table 4. The critical J-integral values were converted to critical elastic-plastic, stress-intensity factors (K_{Jc}), using the plane-strain formulation.

The values of J calculated from the two η-factor techniques are compared to J determined from finite-element analyses for specimens CB-1.1 – CB-1.4 in Fig. 8(a)–(d). In Fig. 8(a), the P vs J curve for CB-1.1 from the finite-element analysis is above the curves generated from toughness estimation techniques. This may be related to the variation of η_{pl} with increasing plastic area for the CB-1.1 specimen, while a constant value of η_{pl} is used in the estimation techniques. For the shallow-crack specimens, there was generally good agreement between experimental and finite-element analysis determined values of J. Although, like CB-1.1, the analysis results exhibited a stiffer response than was indicated from the experimental data.

These data should be regarded as preliminary, since the potential effects of material property gradients in the heat-affected zone (HAZ) (associated with the cladding) were not considered in the toughness determinations.

Residual Stresses

An analytical study was carried out to estimate the effects of residual stresses on measured cleavage fracture toughness data obtained from the full-thickness clad beam specimens CB-1.1 through CB-1.4. A thermal gradient method (TGM) was used to generate stress distributions in the beams that approximate the residual stresses. These estimates of stress distribution were based on previous residual stress studies conducted at

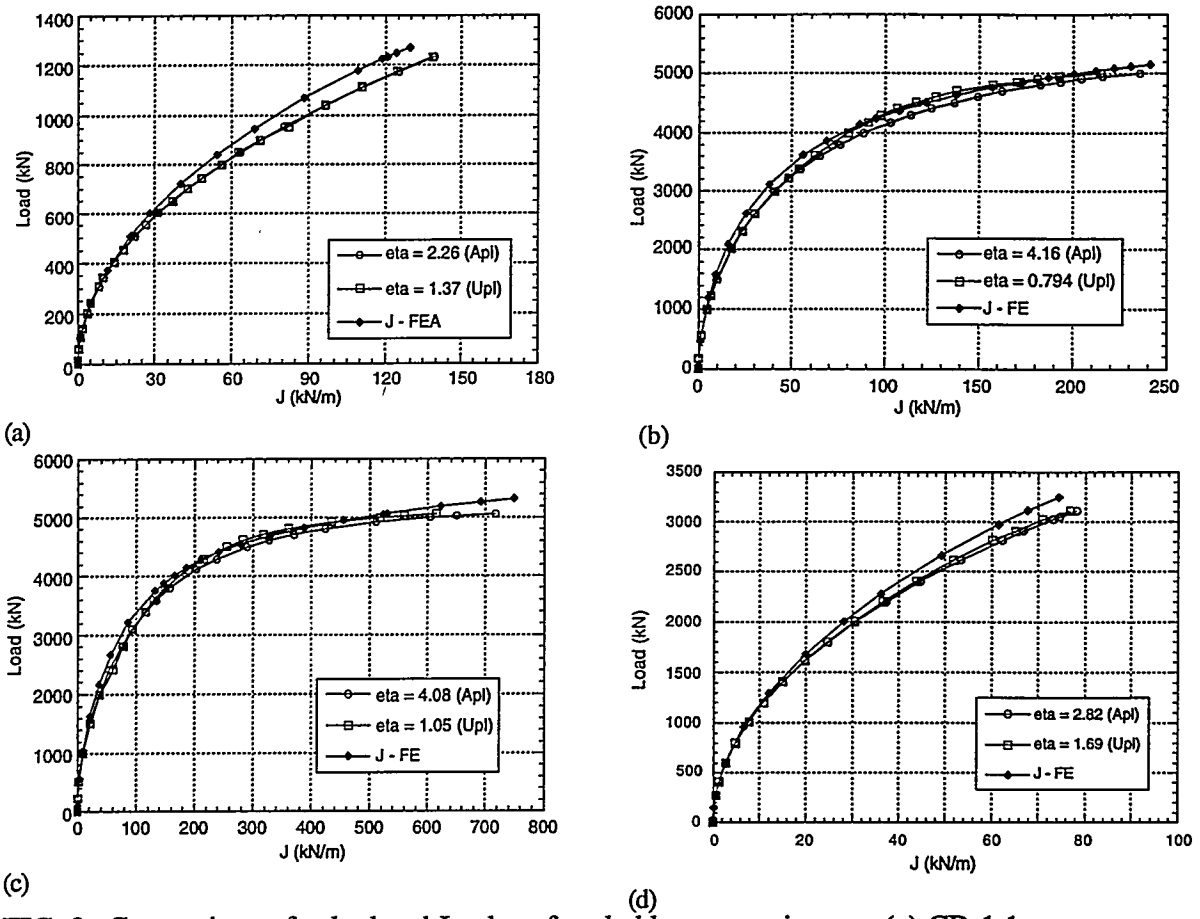

FIG. 8--Comparison of calculated J values for clad beam specimens: (a) CB-1.1, (b) CB-1.2, (c) CB-1.3, and (d) CB-1.4.

ORNL and published in Ref. 17. In the latter studies, the TGM was based on application of a temperature distribution in the form of a cosine function through the thickness of the beam. The temperature distribution was adjusted such that the generated stresses in the beam would cause the opening displacements of a pre-crack notch in the beam to match those recorded during the wire electro-discharge machining of the notch. These fictitious thermal stresses were then imposed as initial stresses on each of the clad beam models containing fatigued through-flaws. It should be noted that residual stress values may be larger in the RPV shell segment from which the clad beam specimens were fabricated. A previous study [18] has shown that the stress level in a specimen cut from a plate is lower than the stress level in the uncut plate, because the stresses in the specimen were allowed to relax when the restraining effects of the plate were removed.

Estimates of residual stress effects on cleavage fracture toughness values measured in each of the four tests are summarized in Table 5. The contribution of the residual stresses to the K-factor applied to the fatigue-sharpened flaw (with no externally applied load) is given in Column (1) of Table 5. Columns (2) and (3) provide estimates of fracture toughness based on CMOD η-factors (Table 4) that exclude and include, respectively, the effects of residual stresses. Residual stresses were shown to have a measurable effect only on the shallow flaw toughness data.

Fracture toughness data from the HSST clad beam and shallow-crack SENB programs are shown in Fig. 9 as a function of normalized temperature (T-NDT). Figure 9 indicates an increase in mean toughness and data scatter with decreased constraint associated with shallow crack testing in the transition temperature region. The range in

scatter for data obtained from the clad beam specimens is consistent with that from the laboratory-scale SENB specimens tested at the same temperature. Note that the minimum toughness value from the clad beam specimens was provided by a shallow-crack beam, not by the single deep-cracked beam tested in this series.

TABLE 5--Summary of residual stress results from the full-thickness clad beam testing program.

Test	a/W	K ($MPa\sqrt{m}$) (1) Residual Stress (RS)	(2) Without RS (η -factors)	(3) With RS (η -factors)
CB-1.1	0.50	6	174	174
CB-1.2	0.05	18	225	243
CB-1.3	0.10	24	393	411
CB-1.4	0.10	24	130	155

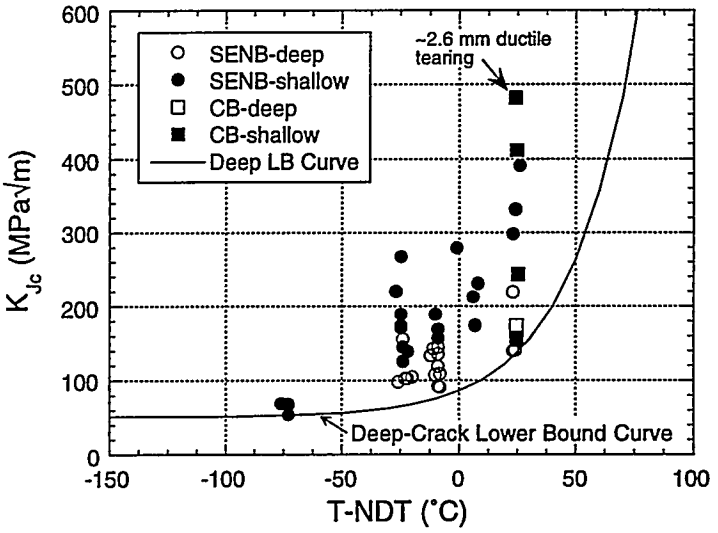

FIG. 9--Fracture toughness as function of normalized temperature T – NDT.

Constraint Analyses

The J-Q methodology [5-7] was used to assess crack-tip stress triaxiality in the clad beam specimens which experienced cleavage initiation. In these analyses, results for the deep-crack specimen (CB-1.1) are employed as an approximation to the small-scale yield (SSY) reference solution. Analyses [4] have shown that $Q \approx 0$ for the deep-crack specimens under these loading conditions. This observation is supported by results shown in Fig. 10(a) for the normalized opening-mode stress (σ_{yy}/σ_0) distributions vs $\tilde{r}$ for the deep-crack specimen CB-1.1. The opening-mode stresses ahead of the crack tip for the shallow-crack specimens, shown in Fig. 10(b), exhibit an essentially uniform deviation from the SSY solution over a distance of $2 \leq \tilde{r} \leq 10$ (i.e., spatially uniform). From Fig.

10(b), the clad beam specimen CB-1.4 has a Q value of about –0.36 at failure (for $\tilde{r} = 2$), whereas CB-1.2 and CB-1.3 had Q values of –0.78 at failure (a significant loss of constraint). This moderate loss of constraint in the CB-1.4 specimen is due primarily to the relatively lower failure load observed in the test.

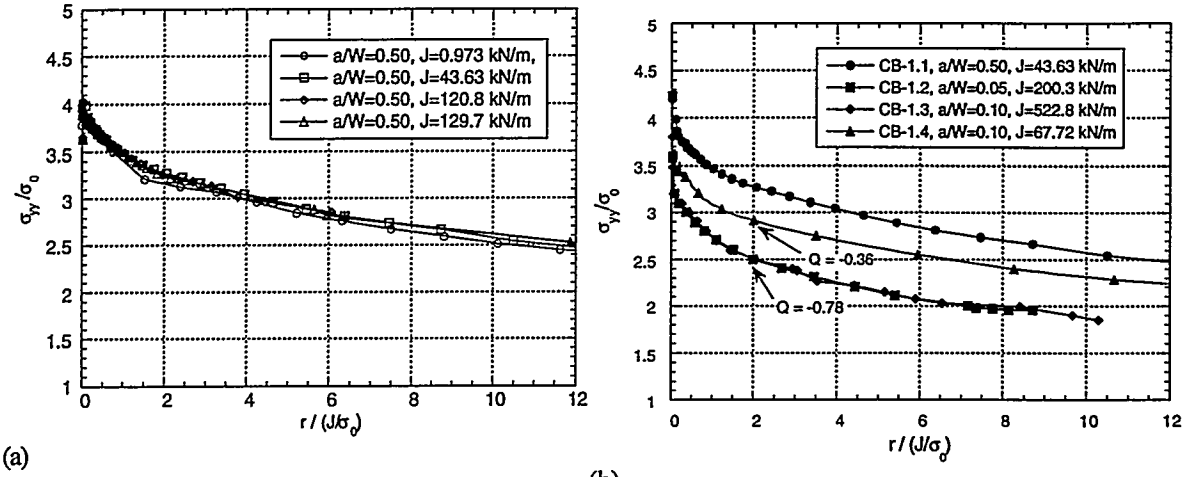

(a) (b)

FIG. 10--Distributions of normalized opening-mode stress for clad beam specimens as a function of applied J: (a) a/W = 0.50, (b) at a/W of 0.50, 0.05, and 0.10.

SUMMARY AND CONCLUSIONS

Beam specimens, which incorporate RPV fabrication welds, base plate, and weld-overlay cladding, are providing fracture toughness data for shallow cracks in material for which metallurgical conditions are prototypic of those found in RPVs. Factors influencing the fracture toughness of RPV material containing shallow cracks include metallurgical gradients, weld inhomogeneities, weld defects, the cladding process, and residual stresses.

In the first testing phase, five full-thickness clad beam specimens were fabricated with through-thickness cracks in weld metal that ranged in depth from 10 to 114 mm ($0.05 \leq a/W \leq 0.5$). These specimens were tested in three-point bending at temperatures in the transition region of the weld metal fracture toughness curve ($T - NDT \approx 25°C$). Fracture toughness estimates were obtained from P vs LLD and P vs CMOD data using finite-element techniques and estimation schemes based on the η-factor method. The cleavage toughness data were compared with other shallow- and deep-crack uniaxial beam data generated previously from A 533 B plate material. Determining conditions in the weld and base metal regions near the cladding is important for interpreting the shallow-crack test results and, consequently, should be included in the HSST Program plan for future work.

These data should be regarded as preliminary, since the potential effects of material property gradients in the HAZ (associated with the cladding deposition) were not considered in the toughness determinations. Material testing is currently underway to study the microstructural variation in the weld and clad HAZ.

In the HSST Program, initial studies of ductile tearing models have focused on the Gurson-Tvergaard (G-T) dilatant plasticity model for void growth and an element extinction capability for modeling crack growth. Two principal input parameters for the G-T model are the initial void volume fraction, f_0, and the characteristic length, D, associated with the G-T crack plane elements. According to theory, these parameters are dependent only on the material and not on specimen geometry. To evaluate this model, plans have been made to generate ductile crack growth data from side-grooved compact tension (CT) specimens taken from the weld material. The parameters f_0 and D will be

calibrated for the material through an iterative process involving finite-element analyses of these CT specimens. The calibrated parameters should provide analytical results in agreement with load versus CMOD and crack growth data from the CT specimens. Values of these parameters from the CT specimen analyses will then be transferred to large-scale structures (for example, the full-thickness clad beams) to determine if they predict the observed response. Metallography may also provide some estimates of initial porosity and inclusion spacing in the weld, which could be compared with values assigned to parameters f_0 and D.

Additional full-thickness clad beams have been tested and results are being evaluated to complete the investigation of fracture toughness of shallow cracks located in prototypical full-thickness plate material. Shallow-crack fracture toughness results from these specimens should provide additional data that are essential to a better understanding of the effects of metallurgical conditions in the region of the clad HAZ.

ACKNOWLEDGMENTS

Research sponsored by the Office of Nuclear Regulatory Research, U.S. Nuclear Regulatory Commission under Interagency Agreement 1886-8011-9B with the U.S. Department of Energy under Contract DE-AC05-96OR22464 with Lockheed Martin Energy Research Corp.

The submitted manuscript has been authored by a contractor of the U.S. Government No. DE-AC05-96OR22464. Accordingly, the U.S. Government retains a non-exclusive, royalty-free license to publish or reproduce the published form of this contribution, or allow others to do so, for U.S. Government purposes.

REFERENCES

[1] W. Marshall et al., "An Assessment of the Integrity of PWR Pressure Vessels," UKAEA Study Group Reports, March 1982.

[2] U. S. Nuclear Regulatory Commission Regulatory Guide 1.154, "Format and Content of Plant-Specific Pressurized Thermal Shock Safety Analysis Reports for Pressurized Water Reactors", January 1987.

[3] R. D. Cheverton and D. G. Ball, Martin Marietta Energy Systems, Inc., Oak Ridge Natl. Lab., "Pressurized-Thermal-Shock Evaluation of the Calvert Cliffs Nuclear Power Plant," pp. 201-244, NUREG/CR-4022, (ORNL/TM-9408), September 1985.

[4] T. J. Theiss, D. K. M. Shum, and S. T. Rolfe, Martin Marietta Energy Systems, Inc., Oak Ridge Natl. Lab., "Experimental and Analytical Investigation of the Shallow-Flaw Effect in Reactor Pressure Vessels," NUREG/CR-5886, (ORNL/TM-12115), July 1992.

[5] N. P. O'Dowd and C. F. Shih, "Family of Crack-Tip Fields Characterized by a Triaxiality Parameter: Part I - Structure of Fields," *J. Mech. Phys. Solids* 39, 989-1015 (1991).

[6] N. P. O'Dowd and C. F. Shih, "Family of Crack-tip Fields Characterized by a Triaxiality Parameter: Part II - Fracture Applications," *J. Mech. Phys. Solids* 40, 939-963 (1992).

[7] N. P. O'Dowd and C. F. Shih, Naval Surface Warfare Center, "Two Parameter Fracture Mechanics: Theory and Applications," USNRC Report NUREG/CR-5958 (CDNSWC/SME-CR-16-92), February 1993.

[8] J. A. Keeney et al., Martin Marietta Energy Systems, Inc., Oak Ridge Natl. Lab., "Preliminary Assessment of the Fracture Behavior of Weld Material in Full-Thickness Clad Beams," NUREG/CR-6228, (ORNL/TM-13091), October 1994.

[9] J. A. Keeney, B. R. Bass, and W. J. McAfee, "Fracture Analysis of Full-Thickness Clad Beam Specimens," Fracture Mechanics: 27th Volume, ASTM STP 1296, Robert S. Piascik, James C. Newman, Jr., and Richard P. Gangloff, Eds., American Society for Testing and Materials, Philadelphia, 1996.

[10] A. L. Gurson, "Continuum Theory of Ductile Rupture by Void Nucleation and Growth: Part I – Yield Criteria and Flow Rules for Porous Ductile Media," Journal of Engineering Materials and Technology, Vol. 99, pp. 2-15, 1977.

[11] *ABAQUS Theory Manual*, Version 5–3, Hibbit, Karlson, and Sorensen, Inc., Providence, R. I., 1993.

[12] K. C. Koppenhoefer, A. S. Gullerud, C. Ruggieri, R. H. Dodds, Jr., and B. E. Healy, Department of Civil Engineering, University of Illinois, "WARP3D: Dynamic Nonlinear Analysis of Solids Using a Preconditioned Conjugate Gradient Software Architecture," UILU-ENG-94-2017, November 1994.

[13] C. Ruggieri and R. H. Dodds, Jr., Department of Civil Engineering, University of Illinois, "Constraint and Ductile Tearing Effects in Statistical Analyses of Cleavage Fracture," UILU-ENG-95-2011, October 1995.

[14] T. J. Theiss et al., Martin Marietta Energy Systems, Inc., Oak Ridge Natl. Lab., "Initial Results of the Influence of Biaxial Loading on Fracture Toughness," NUREG/CR-6036, (ORNL/TM-12349), June 1993.

[15] B. R. Bass et al., Martin Marietta Energy Systems, Inc., Oak Ridge Natl. Lab., "Biaxial Loading and Shallow-Flaw Effects on Crack-Tip Constraint and Fracture Toughness," NUREG/CR-6132, (ORNL/TM-12498), January 1994.

[16] M. T. Kirk and R. H. Dodds, Jr., Department of Civil Engineering, University of Illinois, "J and CTOD Estimation Equations for Shallow Cracks in Single Edge Notch Bend Specimens," USNRC Report NUREG/CR-5969 (CDNSWC/SME-CR-17-92), July 1993.

[17] J. A. Keeney, Martin Marietta Energy Systems, Inc., Oak Ridge Natl. Lab., "Residual Stress Analysis of Full-Thickness Clad Beam Specimens," ORNL/NRC/LTR-94/37), August 14, 1995.

[18] E. F. Rybicki, J. R. Shadley, and A. S. Sandhu, The University of Tulsa, Mechanical Engineering Associates, Inc., "Experimental Evaluation of Residual Stresses in a Weld Clad Plate and Clad Test Specimens," NUREG/CR-4646, MEA-2145, October 1986.

DISCLAIMER